© S. Hirzel Verlag · EAA
ACUSTICA · acta acustica
Vol. 84 (1998) 280–288

Vertical Rail Vibrations: Pointforce Excitation

Anders Nordborg*
The Marcus Wallenberg Laboratory for Sound and Vibration Research, Royal Institute of Technology, S-10044 Stockholm, Sweden

Summary
Fourier transform methods together with Floquet's theorem yield Green's function of the periodically supported rail. The track model includes an infinite Euler-Bernoulli beam, pads with stiffness and damping, flexible sleepers plus a massless ballast with stiffness and damping. The exact analytic solution, in the frequency domain, of the linear differential equation governing rail response, yields a simple, comprehensive and computation efficient tool in sound/vibration optimising track constructions. Laboratory rail receptance measurements were taken on a full-scale piece of stiff-padded rail, resting on 13 ballast-embedded concrete sleepers. Measurements/calculations agree well up to 1800 Hz. The curve fitting provides values of pad/ballast parameters. Rails with broad/pronounced attenuation regions radiate less noise; attenuation, influenced by damping and structural irregularity, increases with pad stiffness, shown by numerical examples. With stiff pads, the attenuation coefficient has local minima near sleeper resonances. The pinned-pinned mode, with minute support motion, propagates through periodically supported rails with any pad stiffness. Finally, it is clearly demonstrated how changed pad stiffness and sleeper spacings alter the receptance, affecting both structure-borne sound and vibrations at the sleeper-passing frequency (50–100 Hz) plus noise generation at the pinned-pinned frequency (around 1000 Hz).

PACS no. 43.40.At, 43.40.Cw, 43.50.Lj

1. Introduction

Advanced track models are motivated by the need to understand, and minimise, noise radiation and structure-borne sound propagation from the track, ballast settlement, pad and clip deterioration, sleeper cracking plus corrugation development. Knothe and Grassie thoroughly review the subject [1].

Remington/Thompson [2, 3, 4] consider wheel-rail rolling noise generation with an infinite continuous rail neglecting the details of the supports. They provide calculated and measured results of vibration decay along the rail; slow decay implies more sound radiation. Grassie *et al.* [5] find, when representing the sleepers as discrete supports, that the pinned-pinned mode strongly affects the rail receptance in the frequency range 600–1000 Hz, for their particular choice of parameters. At the pinned-pinned frequency, a half wavelength equals one sleeper distance, with nodes at the support points. Wave propagation along a periodic structure—a good approximation for a rail-sleeper system—exhibits a stop- and passband behaviour, see e.g. Munjal and Heckl [6] or the book [7] by Cremer, Heckl and Ungar. Maria Heckl finds that wider passbands occur with more than one wave type (vertical/lateral bending plus torsional) present [8, 9]. Another finding is that an irregular distribution of sleepers attenuates waves within passbands, resulting in less noise radiation [10]. Ripke's three-dimensional track model [11] allows for point and cross receptance calculation in the lateral and vertical direction, using a combined finite element and transfer matrix procedure. Curve-fitting calculated receptance curves to those measured is, to date, the only way to determine ballast properties [12]. Ballast stiffness and damping increase with increasing load, yielding a reduced receptance at low frequencies. Mace [13] uses Fourier methods—in principle, the same approach as this paper—to calculate the response of periodically stiffened fluid-loaded plates. He ends up with an exact analytic result.

Here[1], the rail is modelled as an infinite uniform Euler beam resting on identical supports (sleepers) at periodic intervals. Using Fourier transform methods and Floquet's theorem, the obtained solution is the Green's function of the sleeper supported rail, enabling calculation of rail response to all linear types of excitations. Laboratory experiments on an 8.5 m part of a sleeper supported (13 sleepers), ballasted track, validated the transfer function, by curve fitting measured to calculated point receptances, at the same time obtaining appropriate data on ballast and pad parameters. Having validated the new track model, computer simulations provide information about some track parameters' significance. For instance, with stiff pads, sleepers must be modelled as flexible beams; on the other hand, with soft pads a modelling of sleepers as rigid masses suffices. Other sleeper/ballast properties, however, may reduce the importance of sleeper resonances. A tight fastening between rail and sleepers causes practically all waves to be attenuated, apart from the pinned-pinned mode, which can still propagate. The receptance variation through a sleeper span is important for noise and structure-borne sound production. While the variation decreases with soft pads, at the same time propagation regions broaden, contributing to noise production. Reduced receptance variation is also achieved by shorter sleeper spacings plus a stiffer and

Received 21 December 1995,
accepted 23 December 1997.

* Current address: ABB Corporate Research, S-72178 Väterøas, Sweden

[1] This work can also be found in the thesis [14]. Parts were presented at ICA 92 [15].

heavier rail. Decreasing the receptance variation not only slows down corrugation growth [16], but also decreases the high frequency air-borne noise production plus the generation of low-frequency structure-borne sound (if pads are appropriately tuned to the track), shown in a companion paper [17].

2. Theory

2.1. Model Description

2.1.1. Periodically Supported Infinite Beam

The rail is modelled as a uniform Euler beam of infinite length, resting on identical supports (sleepers) at periodic intervals (Figure 1). The complex modulus of elasticity is $E(1 - \mathrm{i}\eta)$, where η is the loss factor, and the moment of inertia of area is I. Thus, the complex bending stiffness is $B = E(1 - \mathrm{i}\eta)I$. The mass per unit length of the beam is m_r, where subscript r denotes rail. The spacing between (the centers of) two sleepers is l. The supports are, here, modelled as lumped mass-spring-damping systems, and have the dynamic stiffness K. The rail is thus restrained to move in the vertical direction by the dynamic stiffness K. No rotational constraints are included. The quantity K contains information about sleeper, ballast and pad (see below) properties. The dynamic stiffness can, in the frequency domain, be written

$$K = K_\mathrm{s} - \omega^2 M_\mathrm{s} - \mathrm{i}\omega C_\mathrm{s}, \tag{1}$$

according to the sign conventions used in this paper (see the definition of the Fourier transform, Section 2.2). The subscript s denotes sleeper. Stiffness K_s, mass M_s, and damping C_s may be frequency dependent, and must in practice be determined by experiments. A track consists of two identical rails, symmetrically connected by sleepers. Because of symmetry, M_s is here half of the sleeper's mass; correspondingly, K_s and C_s are stiffness and damping respectively for a half sleeper.

2.1.2. Inclusion of Pads and Flexible Sleepers

Include a spring K_r with loss factor η_pad between the rail and the sleepers (Figure 2). The dynamic stiffness of the supports changes to

$$K = (K_\mathrm{s} - \omega^2 M_\mathrm{s} - \mathrm{i}\omega C_\mathrm{s}) \cdot \left[\frac{1}{1 + \dfrac{K_\mathrm{s} - \omega^2 M_\mathrm{s} - \mathrm{i}\omega C_\mathrm{s}}{K_\mathrm{r}(1 - \mathrm{i}\eta_\mathrm{pad})}} \right]. \tag{2}$$

Sleeper bending modes influence the dynamic stiffness of the supports. The sleepers are modelled as Euler beams with length l_s and bending stiffness B_s, with loss factor η_s, on a continuously elastic foundation with damping (Figure 3), representing the ballast. Now, M_s is the whole sleeper's mass, since l_s is its whole length; the same applies for K_s and C_s. Introduce the new distributed parameters for sleeper and ballast properties: $M'_\mathrm{s} = M_\mathrm{s}/l_\mathrm{s}$, $C'_\mathrm{s} = C_\mathrm{s}/l_\mathrm{s}$ and $K'_\mathrm{s} = K_\mathrm{s}/l_\mathrm{s}$. Then for a unit force excitation at $z = z_0$ the equation of motion is

$$B_\mathrm{s}\frac{\partial^4 y_\mathrm{s}(z,t)}{\partial z^4} + M'_\mathrm{s}\frac{\partial^2 y_\mathrm{s}(z,t)}{\partial t^2} + C'_\mathrm{s}\frac{\partial y_\mathrm{s}(z,t)}{\partial t} + K'_\mathrm{s} y_\mathrm{s}(z,t) = \delta(z - z_0).$$

The right hand side represents a harmonic unit point force at the position where the rail is fastened to the sleeper. (The factor $\mathrm{e}^{-\mathrm{i}\omega_0 t}$ is omitted because of writing convenience.) A Fourier transform of this equation,

$$B_\mathrm{s} Y_\mathrm{s}^{(iv)}(z) - \omega^2 M'_\mathrm{s} Y_\mathrm{s}(z) - \mathrm{i}\omega C'_\mathrm{s} Y_\mathrm{s}(z) + K'_\mathrm{s} Y_\mathrm{s}(z) = \delta(z - z_0),$$

together with the eight boundary conditions—at $z = \pm l_\mathrm{s}/2$, $Y''_\mathrm{s}(z) = Y'''_\mathrm{s}(z) = 0$; at $z = z_0$, $Y_\mathrm{s}(z)$, $Y'_\mathrm{s}(z)$ and $Y''_\mathrm{s}(z)$ are continuous whereas the third derivative is discontinuous, $Y'''_\mathrm{s}(z + \epsilon) - Y'''_\mathrm{s}(z - \epsilon) = 1/B_\mathrm{s}$ $(\epsilon \to 0)$—uniquely determines the vertical deflection. Thus, the dynamic stiffness

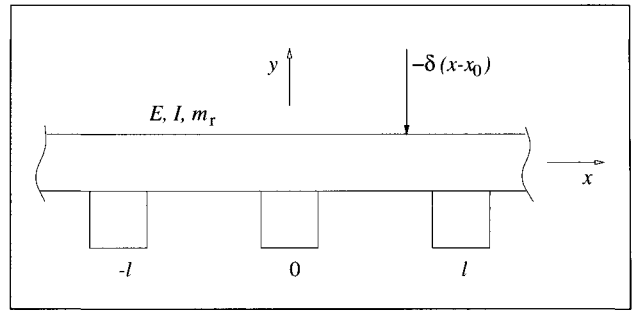

Figure 1. Track model.

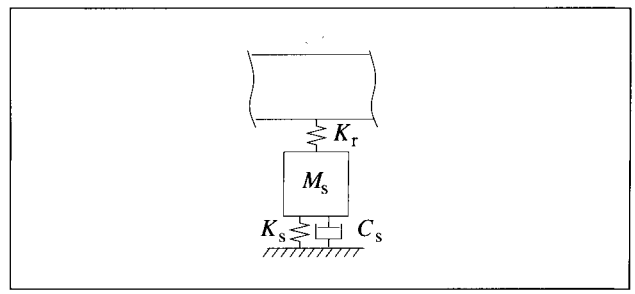

Figure 2. Rail support with pad-sleeper-ballast.

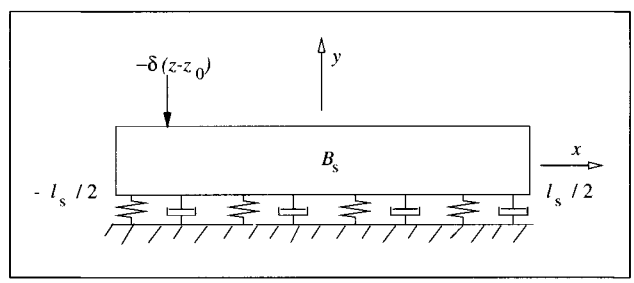

Figure 3. Flexible sleeper on a continuously elastic foundation with damping.

ACUSTICA · acta acustica
Vol. 84 (1998)

of the sleepers at the rail positions is $K_{\text{sleeper}} = Y_{\text{s}}^{-1}(z_0)$; together with rail pads with hysteretic damping resulting in the dynamic stiffness K of the supports, defined by $K^{-1} = [K_{\text{r}}(1 - \mathrm{i}\eta_{\text{pad}})]^{-1} + K_{\text{sleeper}}^{-1}$:

$$K = K_{\text{sleeper}} \left[\frac{1}{1 + \dfrac{K_{\text{sleeper}}}{K_{\text{r}}(1 - \mathrm{i}\eta_{\text{pad}})}} \right]. \tag{3}$$

2.2. Free Vibrations

2.2.1. Fourier Transformation and Floquet's Theorem

Study free vibrations of the rail. Then, the equation of motion is

$$B\frac{\partial^4 y(x,t)}{\partial x^4} + m_{\text{r}}\frac{\partial^2 y(x,t)}{\partial t^2} + \left[K_{\text{s}} y(x,t) + M_{\text{s}}\frac{\partial^2 y(x,t)}{\partial t^2} + C_{\text{s}}\frac{\partial y(x,t)}{\partial t}\right] \cdot \sum_{n=-\infty}^{\infty} \delta(x - nl) = 0, \tag{4}$$

where $y(x,t)$ is the vertical displacement of the rail at the coordinate x, the homogeneous solution. For simplicity, assume that the supports are of the form as of (1). The last term of (4) is a sum of the forces that the supports exert on the rail at the discrete points $x = nl$; the function $\delta(x - nl)$ is the delta function concentrating the supporting forces at points $x = nl$ ($n = 0, \pm 1, \pm 2, \ldots$). After an integration of (4) in the x direction from minus infinity to plus infinity the last term changes to

$$\sum_{n=-\infty}^{\infty} \left[K_{\text{s}} y(nl,t) + M_{\text{s}}\frac{\partial^2 y(nl,t)}{\partial t^2} + C_{\text{s}}\frac{\partial y(nl,t)}{\partial t}\right],$$

after which it is realised that (4) has dimension force per unit length.

Taking an ordinary Fourier transform with respect to time t, defined by

$$y(x,t) = \int_{-\infty}^{\infty} Y(x,\omega)\,\mathrm{e}^{-\mathrm{i}\omega t}\,\mathrm{d}\omega;$$
$$Y(x,\omega) = \frac{1}{2\pi}\int_{-\infty}^{\infty} y(x,t)\,\mathrm{e}^{\mathrm{i}\omega t}\mathrm{d}t,$$

reduces (4) to

$$\frac{\mathrm{d}^4 Y}{\mathrm{d}x^4} - k^4 Y + K' Y \sum_{n=-\infty}^{\infty} \delta(x - nl) = 0, \tag{5}$$

where

$$k = \sqrt[4]{\frac{m_{\text{r}}\omega^2}{B}}; \qquad K' = \frac{K}{B},$$

and

$$K = K_{\text{s}} - \omega^2 M_{\text{s}} - \mathrm{i}\omega C_{\text{s}},$$

agreeing with (1). Now, taking a Fourier transform in the x direction, defined by

$$Y(x) = \frac{1}{2\pi}\int_{-\infty}^{\infty} \hat{Y}(\kappa)\,\mathrm{e}^{\mathrm{i}\kappa x}\,\mathrm{d}\kappa;$$
$$\hat{Y}(\kappa) = \int_{-\infty}^{\infty} Y(x)\,\mathrm{e}^{-\mathrm{i}\kappa x}\,\mathrm{d}x,$$

reduces (5) to

$$\kappa^4 \hat{Y} - k^4 \hat{Y} + K' \sum_{n=-\infty}^{\infty} Y(nl)\mathrm{e}^{-\mathrm{i}\kappa nl} = 0. \tag{6}$$

As (5) can be rewritten as a periodic system with period l, according to Floquet's theorem, the solution is of the form

$$Y(x + nl) = Y(x)\mathrm{e}^{ng}, \tag{7}$$

where g is a coefficient, which may be complex. The proof of this theorem is found in e.g. [18], valid for linear ordinary differential equations of any order. In quantum mechanics, this theorem is also referred to as Bloch's theorem. The basic assumption is that the equation contains some periodic coefficient, i.e. the system is periodic in some sense. The solutions derived with this assumption are valid outside the source region; these solutions are then matched in the source region to satisfy the necessary boundary conditions (see section 2.3). The physical significance of g, the propagation coefficient, is discussed later, under the paragraph 'Dispersion Relation'.

Put $x = 0$ in (7) and substitute this into (6):

$$\hat{Y} = \frac{-K'Y(0)\sum_{n=-\infty}^{\infty} \mathrm{e}^{ng}\mathrm{e}^{-\mathrm{i}\kappa nl}}{\kappa^4 - k^4}.$$

The inverse Fourier transform:

$$Y(x) = -K'Y(0) \sum_{n=-\infty}^{\infty} \{\mathrm{e}^{ng} I_n(x)\}, \tag{8}$$

where

$$I_n(x) = \frac{1}{2\pi}\int_{-\infty}^{\infty} \frac{\mathrm{e}^{\mathrm{i}\kappa(x-nl)}}{\kappa^4 - k^4}\mathrm{d}\kappa. \tag{9}$$

Thus, having evaluated the Fourier integral in (9) and the sum in (8), yields an analytical solution to (5), i.e. the vertical displacement of the rail at any position x and at any wavenumber k (or frequency). As (5) is a fourth-order differential equation, four linearly independent solutions exist. Any linear combination of those is also a solution to the homogeneous equation (5); if there is an exciting force in the right hand side of (5) (see Section 2.3) the constant of each homogeneous solution is determined by matching the boundary conditions in the source region. Putting $x = 0$ in (8) forms a relation between g and k, the dispersion relation. For each value of the wavenumber k four different values of the propagation constant g exist, while for each g there is one linearly independent solution $Y(x)$.

Next, proceed by evaluating the Fourier integral in (9) and the infinite sum in (8).

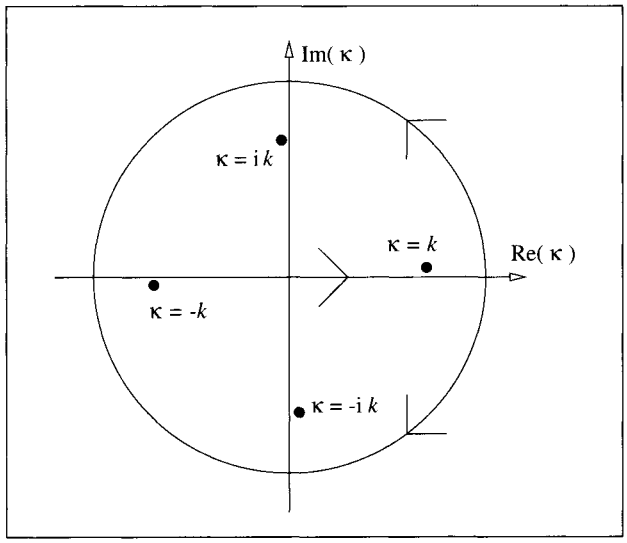

Figure 4. Contour of integration.

2.2.2. Infinite Sum of Fourier Integrals

To evaluate the sum in (8), first evaluate the Fourier integral $I_n(x)$, by residue calculus. Equation (9) can be rewritten

$$I_n(x) = \frac{1}{2\pi}\int_{-\infty}^{\infty} \frac{\mathrm{e}^{\mathrm{i}\kappa(x-nl)}}{(\kappa+k)(\kappa-k)(\kappa+ik)(\kappa-ik)}\mathrm{d}\kappa.$$

This integral is singular for $\kappa = \pm k$. By taking the effects of the structural damping into account [k contains a small positive imaginary part: $k \simeq \Re(k)(1+\mathrm{i}\eta/4))$] the integrand is always finite, and the paths of integration are as shown (see Figure 4). The contour of integration is closed in the upper half-plane for $x \geq nl$ and in the lower half-plane for $x \leq nl$, to ensure convergence of the integral. Residue calculus produces

$$I_n(x) = \frac{1}{4k^3}\begin{cases} \mathrm{i}\mathrm{e}^{\mathrm{i}k(x-nl)} - \mathrm{e}^{-k(x-nl)} & \text{for } x \geq nl, \\ \mathrm{i}\mathrm{e}^{-\mathrm{i}k(x-nl)} - \mathrm{e}^{k(x-nl)} & \text{for } x \leq nl. \end{cases}$$

It is now possible to evaluate the infinite sum in (8). After having done that, see thesis [14], the homogeneous solution, (8), becomes

$$Y(x) = \frac{-K'Y(0)}{4k^3}\left[\frac{\sin k(l-x) + \mathrm{e}^g \sin kx}{\cos kl - \cosh g} - \frac{\sinh k(l-x) + \mathrm{e}^g \sinh kx}{\cosh kl - \cosh g}\right]. \quad (10)$$

This solution is valid only for $0 \leq x \leq l$, because that was assumed when the infinite sum was evaluated. To calculate the response elsewhere, use Floquet's theorem, (7). That the solution fulfills the appropriate boundary conditions at the position $x = l$ is checked in the thesis [14].

It still remains to determine $Y(0)$ and g. As mentioned earlier, $Y(0)$ is fixed by the strength and position of an exciting force (Section 2.3). The propagation coefficient g, on the other hand, depends only on the periodicity of the structure. The relation between the two wavenumbers g and k, the dispersion relation, can be calculated by putting $x = 0$ in (10).

2.2.3. Dispersion Relation

For $x = 0$, (10) reduces to the dispersion relation,

$$\frac{-1}{K'} = \frac{1}{4k^3}\left[\frac{\sin kl}{\cos kl - \cosh g} - \frac{\sinh kl}{\cosh kl - \cosh g}\right]. \quad (11)$$

Two special cases: (i) no vertical displacement is allowed at the supporting points ($K' \to \infty$), the dispersion relation becomes

$$\cosh g = \frac{\cos kl \sinh kl - \cosh kl \sin kl}{\sinh kl - \sin kl};$$

(ii) if the supports are removed ($K' \to 0$), the dispersion relation changes to

$$(\cos kl - \cosh g)(\cosh kl - \cosh g) = 0.$$

The last two equations can also be found in [7], providing a check of the derivation so far. Equation (11) is a second-order equation of $\cosh g$; it can be rewritten

$$\cosh^2 g + \left[\frac{K'}{4k^3}(\sinh kl - \sin kl) - (\cosh kl + \cos kl)\right]\cosh g + \frac{K'}{4k^3}(\cosh kl \sin kl - \cos kl \sinh kl) + \cosh kl \cos kl = 0. \quad (12)$$

This expression was also derived in [6], taking zero rotational inertia of the supports into account. Equation (12) has two solutions for $\cosh g$, but as $\cosh g = \cosh(-g)$ there are four different propagation coefficients $\pm g_{1,2}$ for each wave number k (or frequency). Thus, there are four homogeneous solutions $Y(x)$ [see (10)] to the differential equation (5); the general solution is a linear combination of these four solutions. Actually, (12) has an infinite number of solutions because $\cosh g$ is $2\pi\mathrm{i}$-periodic ($g \pm m2\pi\mathrm{i}$, $m = 0, 1, 2, \ldots$), but since the multiples of g here are all equivalent, put $m = 0$.

The propagation coefficients g are chosen so that $|Y(x)| < \infty$ for $x \to \pm\infty$ ($n \to \pm\infty$) in accordance with Floquet's theorem, $Y(x + nl) = Y(x)\mathrm{e}^{ng}$. Thus, for waves propagating to the right, the propagation coefficient g must not have a positive real part, i.e. $\Re(g_{1,2}^{\text{right}}) \leq 0$, and for waves propagating to the left $\Re(g_{1,2}^{\text{left}}) \geq 0$. Waves decay if $\Re(g) \neq 0$; such frequency ranges are called stopbands. On the other hand, if $\Re(g) \simeq 0$ (some damping is always present), the waves propagate almost unattenuated; these frequency ranges are called passbands.

2.3. Forced Vibrations: Green's Function

Calculate the response, i.e. the vertical rail deflection, at coordinate x due to a stationary harmonic unit point force $\delta(x - x_0)$ at x_0. By definition, the solution is Green's function, $G(x|x_0)$, to the problem stated. Since Green's function here has unit m/N, it is the receptance of the rail. The delta

ACUSTICA · acta acustica
Vol. 84 (1998)

function $\delta(x - x_0)$ concentrates the force at $x = x_0$ (Figure 1). Since the solution must remain finite as $x \to \pm\infty$, only two homogeneous solutions [see (10)] are possible on each side of the force. To the right of the force, these are called Y_1^{r} and Y_2^{r}, with the propagation constants g_1^{r} and g_2^{r}; to the left of the force the solutions are called Y_1^{l} and Y_2^{l}, with the propagation constants g_1^{l} and g_2^{l}. Superscript r denotes right and superscript l denotes left. Green's function is a linear combination of homogeneous solutions:

$$G(x|x_0) = \begin{cases} c_1^{\mathrm{r}} Y_1^{\mathrm{r}} + c_2^{\mathrm{r}} Y_2^{\mathrm{r}} & \text{for } x \geq x_0, \\ c_1^{\mathrm{l}} Y_1^{\mathrm{l}} + c_2^{\mathrm{l}} Y_2^{\mathrm{l}} & \text{for } x \leq x_0. \end{cases}$$

As earlier, this expression is valid for $0 \leq x \leq l$. The four constants c_1^{r}, c_2^{r}, c_1^{l} and c_2^{l}, corresponding to $-Y(0)/4$ from (10), are chosen to match the boundary conditions in the source region. Outside $0 \leq x \leq l$ use Floquet's theorem $Y(x+nl) = Y(x)\mathrm{e}^{ng}$, where $Y = Y_{1,2}^{r,l}$ and the propagation coefficient $g = g_{1,2}^{r,l}$:

$$G(x|x_0) = \begin{cases} c_1^{\mathrm{r}} Y_1^{\mathrm{r}} \mathrm{e}^{ng_1^{\mathrm{r}}} + c_2^{\mathrm{r}} Y_2^{\mathrm{r}} \mathrm{e}^{ng_2^{\mathrm{r}}} & \text{for } n = 1, 2, \ldots, \\ c_1^{\mathrm{l}} Y_1^{\mathrm{l}} \mathrm{e}^{ng_1^{\mathrm{l}}} + c_2^{\mathrm{l}} Y_2^{\mathrm{l}} \mathrm{e}^{ng_2^{\mathrm{l}}} & \text{for } n = -1, -2, \ldots, \end{cases}$$

with the g:s chosen so that $G = G' = 0$ ($' = \mathrm{d}/\mathrm{d}x$) for $x \to \pm\infty$. Integer n is an index associated with a sleeper span. Since the rail is now excited by the unit force $\delta(x - x_0)$, the Fourier transform of the equation of motion of the rail becomes,

$$\mathrm{L}G = \delta(x - x_0), \tag{13}$$

where L is the differential operator

$$\mathrm{L} = B\left[\frac{\mathrm{d}^4}{\mathrm{d}x^4} - k^4 + K' \sum_{n=-\infty}^{\infty} \delta(x - nl)\right]. \tag{14}$$

By integrating (13) four times from $x_0 - \epsilon$ to $x_0 + \epsilon$ ($\epsilon \to 0$) the four boundary conditions at $x = x_0$ are obtained:

$$G^{\mathrm{r}}(x_0) - G^{\mathrm{l}}(x_0) = 0, \tag{15}$$

$$\left(\frac{\mathrm{d}G^{\mathrm{r}}}{\mathrm{d}x}\right)_{x=x_0} - \left(\frac{\mathrm{d}G^{\mathrm{l}}}{\mathrm{d}x}\right)_{x=x_0} = 0, \tag{16}$$

$$\left(\frac{\mathrm{d}^2G^{\mathrm{r}}}{\mathrm{d}x^2}\right)_{x=x_0} - \left(\frac{\mathrm{d}^2G^{\mathrm{l}}}{\mathrm{d}x^2}\right)_{x=x_0} = 0, \tag{17}$$

$$\left(\frac{\mathrm{d}^3G^{\mathrm{r}}}{\mathrm{d}x^3}\right)_{x=x_0} - \left(\frac{\mathrm{d}^3G^{\mathrm{l}}}{\mathrm{d}x^3}\right)_{x=x_0} = \frac{1}{B}. \tag{18}$$

The solution to this system of four linear equations, yields the four constants c_1^{l}, c_2^{l}, c_1^{r} and c_2^{r} (see the thesis [14]). Green's function is now exactly determined. Since Green's function also depends on frequency through the wavenumber k and the dynamic stiffness of the supports K, this is indicated by suffix ω, $G_\omega(x|x_0)$.

3. Results and Discussion

3.1. Rail Receptance Measurements

3.1.1. Results

Laboratory measurements were taken on a full scale piece of track, consisting of two 8.5 m UIC 50 rails laid on 13 concrete sleepers, centre distances $l = 0.65$ m, embedded in a 0.5 m depth of ballast. A hydraulic cylinder applied both a static load and a superimposed dynamic force. Above 200 Hz impacts with a sledge-hammer excited the track.

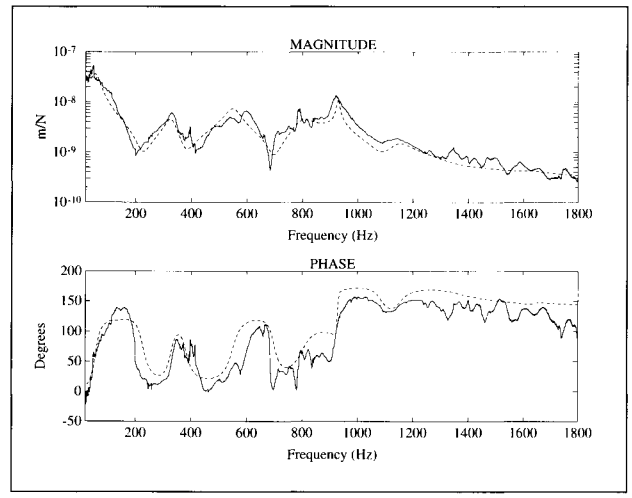

Figure 5. Vertical point receptance of a UIC 50-rail on ballasted concrete sleepers: *solid line*, laboratory measurement: *dashed line*, prediction (curve fit).

The aim of this measurement is to fit calculated (predicted) vertical point receptance of the rail, i.e. Green's function $G_\omega(x_0|x_0)$, to the measured one, according to the theory as described in Section 2.3. In this way, track parameters such as ballast properties are determined. For the calculation, parameters according to Table I, as defined in Section 2.1 are used. The value of the moment of inertia I, which is used in the calculations is about 75 % of the tabulated value ($20.45 \cdot 10^{-6}$ m^4) for a UIC 50-rail, providing the simplest possible mean to compensate for frequency limitations of the Euler-Bernoulli beam theory. Sleeper and ballast properties M_{s}, C_{s} and K_{s} apply to a whole sleeper length, in accordance with the discussion preceeding (3); corresponding values per unit length are $M_{\mathrm{s}}' = 100$ kg/m, $C_{\mathrm{s}}' = 22 \cdot 10^3$ Ns/m^2 and $K_{\mathrm{s}}' = 17 \cdot 10^6$ N/m^2. These particular ballast parameters apply to the preload 25 kN (per wheel). Hysteretic pad damping, viscous ballast damping plus flexibly modelled sleepers [see (3)] yield a high degree of agreement between predictions and measurements (Figure 5) for the point receptance between two sleepers ($x_0/l = 0.5$) up to 1800 Hz. Both measurement and calculation show resonances around a number of frequencies: 50, 320, 600, 800, 930 and 1150 Hz.

3.1.2. Discussion

Figure 5 shows measured with calculated point receptance of the rail in the middle of a sleeper span. A reduction of the moment of inertia of the rail by some 25 % from the tabulated value, moves the pinned-pinned frequency down from about 1090 Hz to 930 Hz, thus extending the region where the Euler-Bernoulli beam model of the rail is useful. The agreement calculations *vs.* experiments is excellent at high as well as low frequencies, where support stiffness is the key parameter. A frequency-dependent bending stiffness

Table I. Track parameters for calculations.

	Value	Description
E	$2.1 \cdot 10^{11}$ N/m^2	rail modulus of elasticity
η	0.004	rail loss factor
I	$15.45 \cdot 10^{-6}$ m^4	rail moment of aerea inertia
m_r	52 kg/m	rail mass per length
l	0.65 m	sleeper spacing
K_r	$500 \cdot 10^6$ N/m	pad stiffness
η_{pad}	0.15	pad loss factor
l_s	2.5 m	sleeper length
M_s	250 kg	sleeper mass
M_s'	100 kg/m	sleeper mass per length
B_s	$4.6 \cdot 10^6$ Nm^2	sleeper bending stiffness
η_s	0.01	sleeper loss factor
K_s	$42.5 \cdot 10^6$ N/m	ballast stiffness
K_s'	$17 \cdot 10^6$ N/m^2	ballast stiffness per length
K_s'	$60 \cdot 10^6$ N/m^2	the same, for Secs. 3.2–3.3
C_s	$55 \cdot 10^3$ Ns/m	ballast damping
C_s'	$22 \cdot 10^3$ Ns/m^2	ballast damping per length
C_s'	$60 \cdot 10^3$ Ns/m^2	the same, for Secs. 3.2–3.3
z_0	-0.75 m	sleeper excitation point

or a Timoshenko beam would of course be more appropriate; compared with a Timoshenko beam, however, the approximation used in this paper produces almost the same results regarding dispersion relations and receptances [19]. Also bear in mind that now only the general vibrational behaviour of the track is explored, representing the sleepers as discrete supports, as opposed to oversimplified modellings (e.g. [4]), neglecting support details.

Ballast becomes stiffer as it is compressed, resulting in lower receptance in the low-frequency region, where ballast movement determines track behaviour. In the receptance plot, rail and sleepers resonance moving in phase on the stiffness of the ballast occurs around 50 Hz. Other authors, e.g. [12], try to improve the curve-fit of predictions to measured data at low frequencies by adding extra mass to the sleepers in their calculations. Particular interest in non-linear ballast behaviour justifies an elaborate modelling and investigation of that element of the track. The aim here, however, is to describe the general behaviour of the track simply modelled with as few elements as possible.

The different resonances of the receptance plot have the following meanings: around 50 Hz, rail and sleepers move in phase on the stiffness of the ballast (ballast resonance); around 320 Hz, the sleepers have their second (asymmetric) bending mode; around 600 Hz, the sleepers have their third (symmetric) bending mode; around 800 Hz, rail and sleepers move out of phase with the stiffnesses of the pads between them (pad resonance); around 930 Hz, the rail vibrates in its pinned-pinned mode (f_{pp}), with node points at the sleeper positions and a half bending wavelength in between; finally, around 1150 Hz the sleepers have their fourth (asymmetric) bending mode. The calculated resonance at the pinned-pinned frequency becomes narrower than the measured, possibly because the sleeper distances of the real track are irregular, or rail fasteners are, in the model, represented by point rather than distributed connections. The importance

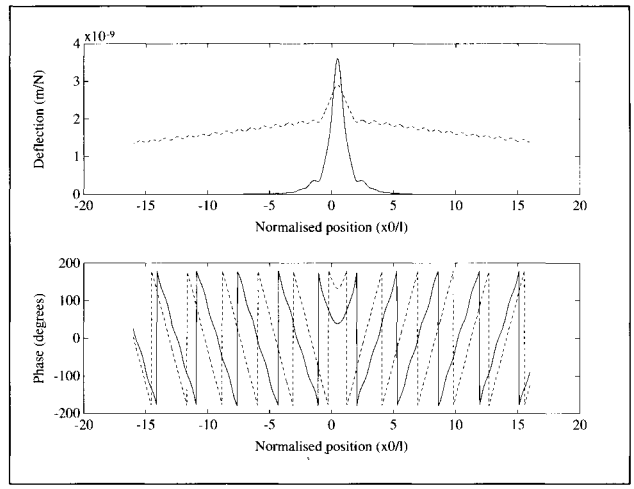

Figure 6. Propagation of vibrations through rail-sleeper system: excitation frequency $f_0 = 500$ Hz; excitation position $x_0/l = 0.5$; *solid line*, $K_r = 500$ MN/m; *dashed line*, $K_r = 60$ MN/m.

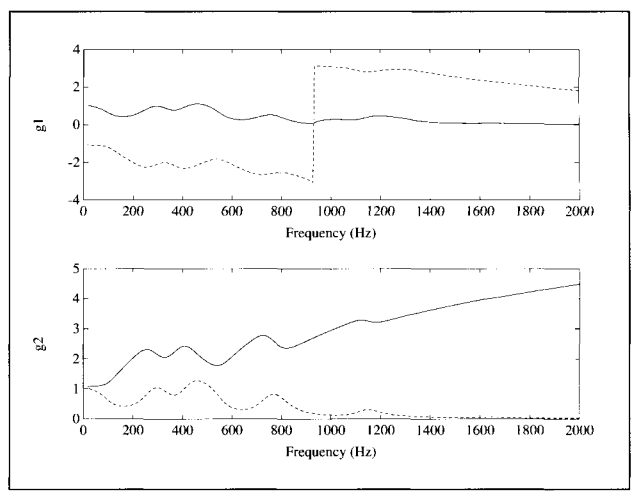

Figure 7. Propagation coefficients for rail-sleeper system with stiff pads, $K_r = 500$ MN/m: *solid line*, real part; *dashed line*, imaginary part.

of including the sleeper flexibility in a track model using stiff pads should be clear by now. However, with soft pads the situation is quite different (see Section 3.3).

3.2. Dispersion Relation Calculations

The propagation curves (Figure 6), or transfer functions, are calculated by Green's function as defined by (13), and the dispersion relation curves (Figures 7, 8 and 9) by (12). The rail parameters are assumed to be the same as those in Section 3.1.1, apart from the ballast properties, assuming instead a 100 kN preload (per wheel), yielding ballast stiffness $K_s' = 60$ MN/m^2 and damping $C_s' = 60$ kNs/m^2. Since the pad stiffness is a parameter which is relatively easy to change in practice, results for rails on stiff pads, $K_r = 500$ MN/m, and on soft pads, $K_r = 60$ MN/m, are compared to illuminate the vibrational properties of each.

ACUSTICA · acta acustica
Vol. 84 (1998)

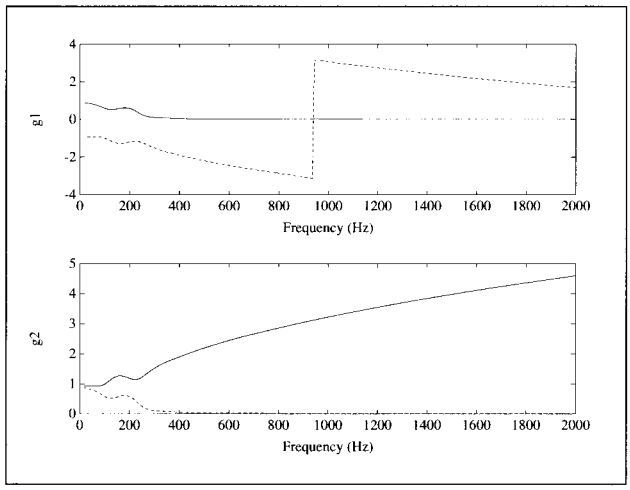

Figure 8. Propagation coefficients for rail-sleeper system with soft pads, $K_r = 60$ MN/m: *solid line*, real part; *dashed line*, imaginary part.

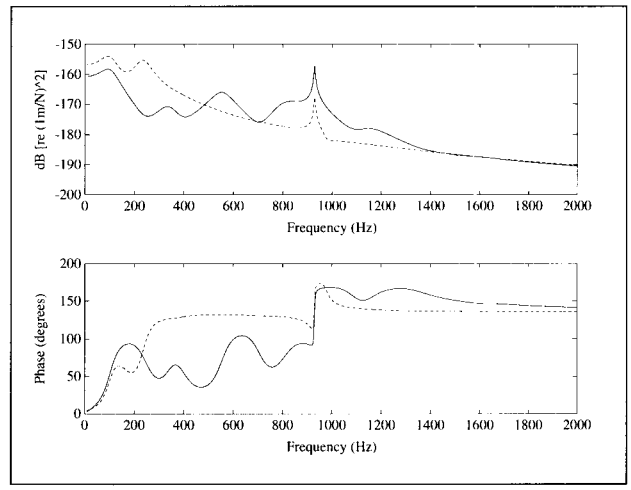

Figure 10. Vertical point receptance spectra for rail at $x_0/l = 0.5$: *solid line*, $K_r = 500$ MN/m; *dashed line*, $K_r = 60$ MN/m.

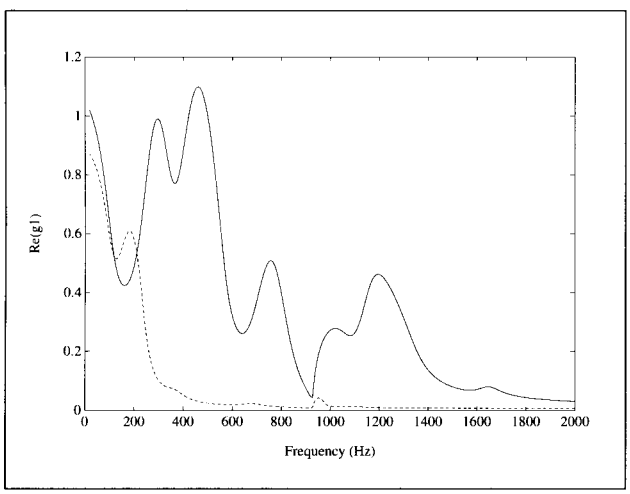

Figure 9. Attenuation coefficients for rail-sleeper system with stiff and soft pads: *solid line*, $K_r = 500$ MN/m; *dashed line*, $K_r = 60$ MN/m.

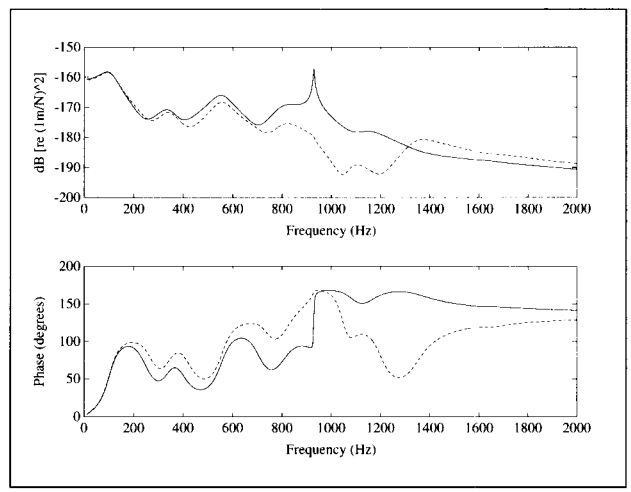

Figure 11. Vertical point receptance spectra for rail with stiff pads, $K_r = 500$ MN/m: *solid line*, $x_0/l = 0.5$; *dashed line*, $x_0/l = 0$.

In stopbands, the propagation coefficient has a positive real part, $\Re(g_1) > 0$ [see the discussion following (12)]; in passbands, $\Re(g_1) = 0$. Pass- and stopband properties apply to undamped periodic systems; for damped cases, propagation/attenuation regions are more appropriate. Since $\Re(g_2) > 0$ always, the near field only exists near the excitation force (Figures 7 and 8). By definition, the attenuation of rail vibration per sleeper span is $e^{-\Re(g_1)}$ [mostly some bays away from the excitation force, where the near field has decayed (Figure 6)].

Vibrations propagate away from the force more easily in a rail-sleeper system with soft pads for which the rail is uncoupled from the sleepers over a broad frequency range (Figure 6). Attenuation regions are more pronounced for the system with stiff pads (Figures 7, 8 and 9). For stiff pads, the attenuation coefficient has local minima near sleeper resonances (compare Figures 9 and 10 plus reference [20]). All rails have propagation regions around the pinned-pinned frequency, with minute support motion, though increased attenuation occurs with stiff pads (Figure 9).

Stop- and passband properties (no damping assumed) are a consequence of the periodicity of the rail-sleeper system. When this periodicity is disturbed, wave propagation is impeded [10], resulting in less noise radiation.

3.3. Rail Receptance Calculations

The example in Figure 10 shows the calculated point receptance of a stiffly padded rail with a softly padded, where parameters are chosen according to Table I. With stiff pads, the receptance curve exhibits resonances around 100, 350, 550, 800, 930 and 1150 Hz; whereas the curve for soft pads has resonances only around 100, 250 and 930 Hz. Section 3.1.2 explains the physical significance of the resonances.

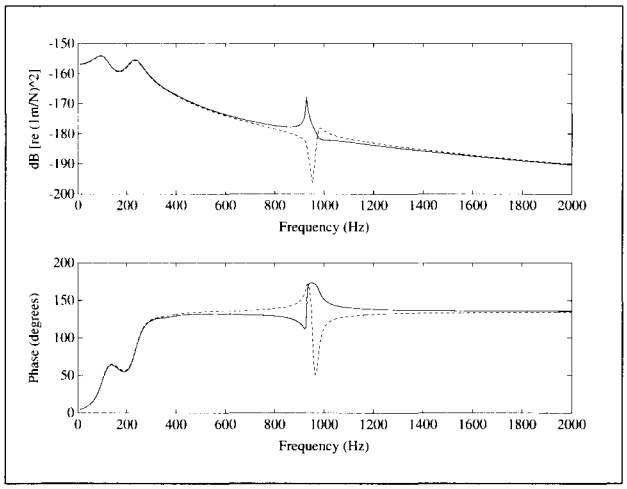

Figure 12. Vertical point receptance spectra for rail with soft pads, $K_r = 60$ MN/m: *solid line*, $x_0/l = 0.5$; *dashed line*, $x_0/l = 0$.

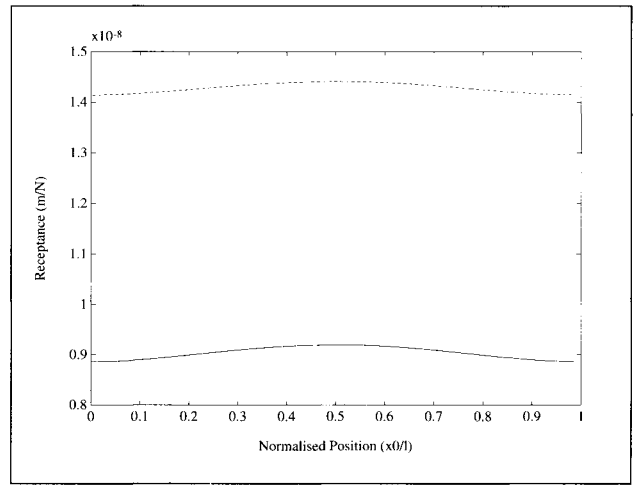

Figure 14. Receptance variation for a static load, $f_0 = 0$ Hz, through a sleeper span for rail: *solid line*, $K_r = 500$ MN/m; *dashed line*, $K_r = 60$ MN/m.

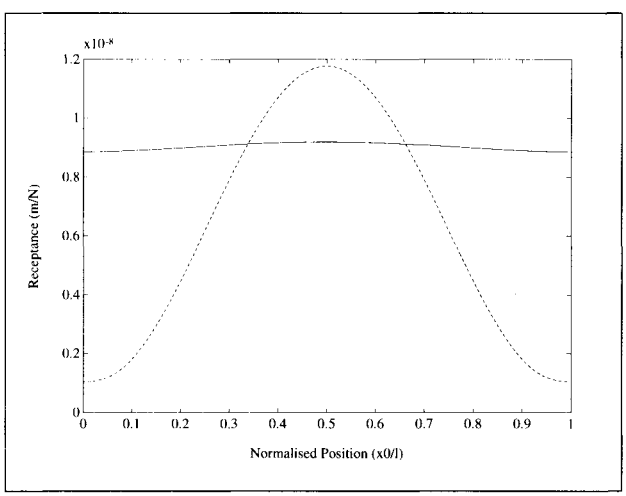

Figure 13. Receptance variation through a sleeper span for rail with stiff pads, $K_r = 500$ MN/m: *solid line*, $f_0 = 0$ Hz; *dashed line*, $f_0 = f_{pp} = 930$ Hz.

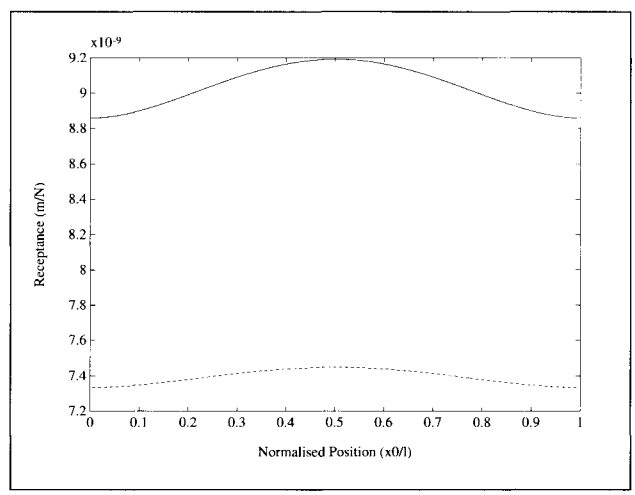

Figure 15. Receptance variation for a static load, $f_0 = 0$ Hz, through a sleeper span for stiffly padded rail: *solid line*, $l = 0.65$ m; *dashed line*, $l = 0.5$ m.

Soft pads move the pad resonance down to about 250 Hz, isolating the rail from the movements of the sleepers; sleeper modes do not appear in the receptance curve for the soft-padded rail. Changing pads however, does not change the appearance of the receptance curve between two sleepers above 1400 Hz, where bending stiffness and rail mass determine vibrational behaviour. Rail response increases with pad stiffness in the region 500–1400 Hz (for the chosen parameters), with more pronounced pad, pinned-pinned mode and sleeper resonances.

Around the pinned-pinned frequency f_{pp} with a peak at 930 Hz (Figure 10), the receptance is higher between two sleepers than precisely above one (Figures 11 and 12). Right above a sleeper position, the pinned-pinned mode, with nodes at the sleeper positions, is hard to excite. Receptance varies through a sleeper span, in particular around the pinned-pinned frequency f_{pp}, equally for a static load (Figure 13). Stiff pads broaden the frequency range around the pinned-pinned frequency with a great receptance variation (compare Figures 11 and 12). The variation causes generation of low frequency noise and vibration, at the sleeper-passing frequency f_s, i.e. around 100 Hz for high speed trains (see companion paper [17]); and noise generation at the pinned-pinned frequency f_{pp}, around 1000 Hz, due to modulation of the contact force [17]. Softer pads and shorter sleeper distances, for instance, reduce the receptance variation (Figures 14 and 15); altered sleeper distance, however, also implies another sleeper-passing f_s and pinned-pinned frequency f_{pp}.

4. Conclusions

The exact analytic solution, in the frequency domain, of the linear differential equation governing rail response, yields a simple, comprehensive and computation efficient tool in sound/vibration optimising track constructions. Rail recep-

tance measurements/calculations show a clear sleeper resonance dependence. Rails with broad/pronounced attenuation regions radiate less noise; attenuation, influenced by damping and structural irregularity, increases with pad stiffness. With stiff pads, the attenuation coefficient has local minima near sleeper resonances. The pinned-pinned mode, with minute support motion, propagates through all (any pad stiffness) periodically supported rails. Softer pads and shorter sleeper spacings reduce the receptance variation through the sleeper spans, affecting both structure-borne sound and vibrations at the sleeper-passing frequency (50–100 Hz) plus noise generation at the pinned-pinned frequency (around 1000 Hz).

Acknowledgement

Swedish Transport & Communications Research Board (KFB) supported the project, running January '90 – June '95. Thanks are also due to all my colleagues at The Marcus Wallenberg Laboratory for Sound and Vibration Research; and at Institut für Technische Akustik, Technische Universität Berlin.

With special thanks to Professor Anders Nilsson, MWL.

References

[1] K. Knothe, S. L. Grassie: Modelling of railway track and vehicle/track interaction at high frequencies. Vehicle System Dynamics **22** (1993) 209–262.

[2] P. J. Remington: Wheel/rail rolling noise, I: Theoretical analysis. Journal of the Acoustical Society of America **81** (1987) 1805–1823.

[3] P. J. Remington: Wheel/rail rolling noise, II: Validation of the theory. Journal of the Acoustical Society of America **81** (1987) 1824–1832.

[4] D. J. Thompson: Wheel-rail noise generation, part III: Rail vibration. Journal of Sound and Vibration **161** (1993) 421–446.

[5] S. L. Grassie, R. W. Gregory, D. Harrison, K. L. Johnson: The dynamic response of railway track to high frequency vertical excitation. Journal Mechanical Engineering Science **24** (1982) 77–90.

[6] M. L. Munjal, M. Heckl: Vibrations of a periodic rail-sleeper system excited by an oscillating stationary transverse force. Journal of Sound and Vibration **81** (1982) 491–500.

[7] L. Cremer, M. Heckl, E. E. Ungar: Structure-borne sound. Second ed. Springer-Verlag, 1988.

[8] M. A. Heckl: Coupled waves on a periodically supported Timoshenko beam. Report to the ORE (now ERRI) Committee C 163 Department of Mathematics, Keele University, Keele, U.K., 1992.

[9] M. A. Heckl: Anregung von gekoppelten Wellen auf einem Timoshenko-Balken mit äqudistanten Stützstellen. DAGA 92-Berlin, 1992. 1033–1036.

[10] M. A. Heckl: Schallabstrahlung von Gleisen mit unregelmäßigen Schwellenabständen. DAGA 94-Dresden, 1994. 317–320.

[11] B. Ripke: Hochfrequente Gleismodellierung und Simulation der Fahrzeug-Gleis-Dynamik unter Verwendung einer nichtlinearen Kontaktmechanik. Dissertation. Technische Universität Berlin, 1994. Fortschritt-Berichte VDI Reihe 12 Nr. 249.

[12] B. Ripke: Anpassung der Modellparameter eines Gleismodells an gemessene Gleisrezeptanzen. ILR Mitteilung 274, Institut für Luft- und Raumfahrt, Technische Universität Berlin, 1992.

[13] B. R. Mace: Periodically stiffened fluid-loaded plates, I: Response to convected harmonic pressure and free wave propagation. Journal of Sound and Vibration **73** (1980) 473–486.

[14] A. Nordborg: Vertical Rail Vibrations: Noise and Structure-Borne Sound Generation. Dissertation. Kungl Tekniska Högskolan, Stockholm, 1995.

[15] A. Nordborg: Rail receptance. 14th International Congress on Acoustics - Bejing, September 1992.

[16] K. Hempelmann: Short pitch corrugation on railway rails: A linear model for prediciton. Dissertation. Technische Universität Berlin, 1994.

[17] A. Nordborg: Vertical Rail Vibrations: Parametric Excitation. ACUSTICA — acta acustica **84** (1997) 289–300.

[18] Coddington, Levinson: Theory of ordinary differential equations. McGraw-Hill, 1955.

[19] J.-F. Hamet: Bruit ferroviaire—Propagation des ondes de flexion d'un rail posé sur traverses: Modèles d'Euler et de Timoshenko. Tech. Rept. MMA 9704, INRETS, 69675 Bron Cedex, France, 1997.

[20] M. Heckl: Wave propagation on beam-plate systems. The Journal of the Acoustical Society of America **33** (1961) 640–651.